Check for updates

Rapid and selective adsorption of a typical aromatic organophosphorus flame retardant on MIL-101-based metal–organic frameworks†

Hui Su, Jiaxin Lv, Liansheng Yang, Li Feng, Yongze Liu, Ziwen Du* and Liqiu Zhang ⬤ *

The pollution of aromatic organophosphorus flame retardants (aromatic OPFRs) in aquatic environments has drawn great attention over the last few years. Two MIL-101-based metal–organic frameworks (Cr-MIL-101 and Fe-MIL-101-NH$_2$) which possess ordered mesoporous cavities (2.9 and 3.4 nm) and aromatic structures were chosen and prepared to selectively adsorb a typical aromatic OPFR [triphenyl phosphate (TPhP)] from aqueous solution. Pore distribution analysis showed that Cr-MIL-101 and Fe-MIL-101-NH$_2$ had both a mesoporous structure (2–3.5 nm) and microporous structure (1–2 nm), conducive to diffusion and adsorption of TPhP molecules. Compared with Fe-MIL-101-NH$_2$ as well as commercial activated carbon, Cr-MIL-101 showed rapid and efficient adsorption for TPhP, and its initial sorption velocity (v_0) calculated from the pseudo-second-order model was up to 568.18 μmol g^{-1} h^{-1}. The adsorption equilibrium of TPhP on the Cr-MIL-101 was almost achieved within 12 h, while the equilibrium time of other adsorbents required more than 48 h. The study of selective adsorption found that Cr-MIL-101 had a higher sorption amount for aromatic OPFRs than alkyl-OPFRs and other aromatic compounds with different chemical structures. Cr-MIL-101 was able to keep a steady selective adsorption for TPhP in the presence of co-existing aromatic compounds. Based on the analysis of K_{ow}, molecular structure and further density functional theory calculations, hydrophobic interactions may play a dominant role in the selective adsorption process of TPhP, and π–π interactions may be also involved. Cr-MIL-101 exhibits reusability and promising potential to rapidly and selectively remove aromatic OPFR in environmental remediation.

Introduction

With the widespread use of synthetic materials, such as plastics, and the development of stringent fire protection standards, the application of flame retardants is increasing significantly. The demand for organophosphorus flame retardants (OPFRs) which are new alternatives for traditional brominated flame retardants is continuing to increase.[1] The global consumption proportion of OPFRs has increased from 16% in 2013 to 18% in 2016, with an average annual consumption of 4.05 × 10^6 tons.[2] Among OPFRs, aromatic OPFRs are ubiquitous in water environments[3,4] and easier to be further enriched on solid surfaces such as soil and organisms[5] due to their relatively higher hydrophobicity, leading to extra pollution and health risks. Triphenyl phosphate (TPhP) which is most frequently detected aryl-OPFR

in the environment[6] is widely used in various aspects of life. Besides as a flame retardant, TPhP is also added in cosmetic products as an elasticizer. TPhP has been detected in several different water bodies such as wastewater, groundwater, oceans and drinking water around the world.[3,7] The concentration of TPhP in surface water was found to be able to reach about 14 000 ng L^{-1} in Norway.[6] TPhP has the longest half-life among OPFRs[2] and can persist in water for 5.5 years under neutral condition. Toxicological research found that TPhP has reproductive toxicity,[6] carcinogenicity[8] as well as chronic toxicity,[9] and may lead to biological genetic defects.[6] Due to its toxicity and potential risks, such OPFR has been listed as a highly concerned pollutant by European Union and United States.[10]

However, since aromatic OPFR is a new type of emerging pollutant, reports on this substance mainly focus on the investigation in different environmental mediums, as well as the establishment of analytical methods, environmental hazards and toxicity analysis. To date, only a few studies regarding the removal of aromatic OPFRs from aquatic environments have been reported. Some degradation techniques such as using acclimatized electrode biofilm[11] and activated peroxymonosulfate (or persulfate) oxidation[12] exhibited efficient TPhP removal from water environment, but the

Beijing Key Laboratory for Source Control Technology of Water Pollution, Engineering Research Center for Water Pollution Source Control and Eco-remediation, College of Environmental Science & Engineering, Beijing Forestry University, 35 Tsinghua East Road, Beijing 100083, China. E-mail: ziwendu@bjfu.edu.cn; zhangliqiu@163.com; Tel: +86-10-62336246

† Electronic supplementary information (ESI) available. See DOI: 10.1039/c9ra09062b

degradation decreased as the co-existing ions existed and the major products were found to be other types of aromatic OPFRs like diphenyl phosphate (DPhP) and hydroxyl triphenyl phosphate (OH-TPhP).[11] Studies have shown that the removal of aromatic OPFRs by adsorption technology is a potentially effective method, but limited reports have been published.[13,14] Yan et al.[15] found that the removal of aromatic OPFRs from water by carbon nanotubes was higher than that of alkyl-OPFRs, which might be attributed to the stronger hydrophobic interactions and $\pi-\pi$ interactions. It was reported that the adsorption capacity of porous polymer adsorbents (resins) could reach about 400 μmol g^{-1} with the TPhP initial concentration of 2.5 μmol L^{-1}. However, the adsorption equilibrium time of resins required at least 192 h, and the removal of TPhP was significantly influenced by the competition from the co-existing organic matters.[16] Therefore, the study of efficient, especially rapid and selective, adsorption for TPhP is very important, and exploring the adsorbent with above performance is a critical challenge.

Metal–Organic Frameworks (MOFs) are organic–inorganic hybrid porous materials assembled from metal ions or metal clusters and organic ligands. MOFs have the advantages of high specific surface area, high and adjustable porosity, diverse structural composition, hydrophobic benzene structures, etc. They were used for adsorption of gaseous substance first and then have been applied to adsorb pollutants from water in recent years.[17,18] MIL series of MOF materials are formed by coordination of metal ions such as Al^{3+}, Cr^{3+} and Fe^{3+} with dicarboxylic acid ligand in a benzene-containing compound. Compared with other types of MOFs, the materials of MIL series possess higher stability in water environment and nanopores at the range of about 1–4 nm (ref. 19) which may be conducive to the sorption of TPhP molecules whose maximum molecular diameter is about 1.14 nm (calculated by Gaussian 09 software). Besides, the benzene structures in such MOFs can form $\pi-\pi$ interactions with aromatic substances.[20] It have been reported that some flame retardants can be encapsulated in MOFs,[21,22] but the amount of relevant studies is still limited. Li et al.[23] found that MIL-based MOFs showed the effective adsorption of a typical brominated flame retardant, hexabromocyclododecane, from aquatic environment via hydrophobic interactions. Accordingly, MIL-based MOFs probably have potential for efficient removal of aromatic OPFRs. MOFs have been more widely studied and applied in water treatment techniques over the last few years,[24,25] but whether MOFs are effective and selective for the removal of aromatic OPFRs from aquatic environments is unclear.

The objectives of the study are to prepare MIL-101 who has mesoporous cavities (2.9 and 3.4 nm) as a high-efficiency adsorbent for the removal of a typical aromatic OPFR, TPhP, and to elucidate the adsorption behaviors as well as mechanisms. The MIL-101 materials were synthesized by hydrothermal method, and the structure of materials was characterized. The adsorption kinetics, isotherms, and the effects of solution pH, inorganic salts as well as co-existing organic compounds including other types of OPFRs and common aromatic pollutants on TPhP adsorption were investigated, and the selective adsorption mechanisms using density functional theory (DFT) calculations were also studied and proposed. Finally, the adsorbent reusability and regeneration were evaluated.

Materials and methods

Chemicals and materials

Chromic chloride hexahydrate, iron(III) chloride hexahydrate, sodium hydroxide, sodium chloride, calcium chloride and N,N-dimethylformamide (DMF, 98%) were purchased from Sinopharm Chemical Reagent Co., Ltd. (Shanghai, China). The terephthalic acid (H$_2$BDC, 99%), 2-aminoterephthalic acid (H$_2$BDC-NH$_2$, 99%), bezafibrate (>97%), phenol (>99%) and 2,4,6-trimethylphenol (>98%) were purchased from Aladdin Reagent Co., Ltd. (Shanghai, China). TPhP (99%) was purchased from Micxy Reagent Co., Ltd. (Chengdu, China), and its molecular structure was shown in Fig. 1. Tris(2-chloroethyl) phosphate (TCEP, 99%), tris(1-chloro-2-propyl) phosphate (TCPP, 99%), tri-isobutyl phosphate (TiBP, 99%) and DPhP (99%) were also purchased from Micxy Reagent Co., Ltd. (Chengdu, China), and the physicochemical properties of above compounds are shown in Table S1.†

Preparation of adsorbent material

In this study, Cr-MIL-101 material was synthesized by hydrothermal method.[26] First, 1.33 g of CrCl$_3$·6H$_2$O (5.0 mmol) and 0.83 g of H$_2$BDC (5.0 mmol) were added into 36 mL of deionized water and mixed for 30 min under sonic vibration to make the solute evenly dispersed. The solution was transferred to a reaction kettle and placed in a muffle furnace previously heated to 100 °C, and then reacted at 210 °C for 24 h. After the reaction was completed, the solution was centrifuged at 8000 rpm for 10 min, and the supernatant was discarded to obtain a green precipitate. The green precipitate was washed using DMF for three times, and each washing was conducted for 3 h to remove unreacted H$_2$BDC. The residual DMF was then removed by ethanol. Finally, the green mixture was vacuum dried and ground into powder, which is the Cr-MIL-101 adsorbent prepared via the above procedure.

Fe-MIL-101-NH$_2$ material was also prepared by hydrothermal method.[27] The specific procedure is as follows: 811.5 mg of FeC1$_3$·6H$_2$O (3.0 mmol) and 543 mg of H$_2$BDC-NH$_2$ (3.0 mmol)
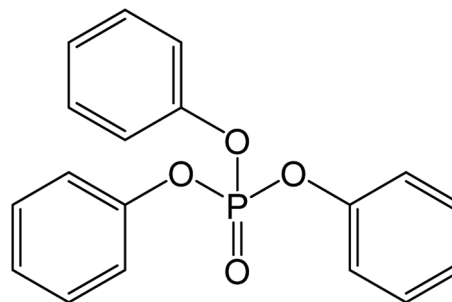

Fig. 1 TPhP molecular structure.

were dissolved in DMF solution. After fully dissolved, the mixture was transferred to the reactor and placed in a muffle furnace which was pre-heated to 120 °C for 10 h at constant temperature. After hydrothermal reaction, the product was centrifugally separated from DMF solvent, and then the solid product was washed with DMF for several times to remove the residual impurities. Then the product was stirred for 3 h in methanol at 60 °C in water bath, then filtered and separated, and the product was washed again using methanol. Finally, the washed product was vacuum dried and ground into powder, which is the Fe-MIL-101-NH$_2$ adsorbent.

Characterization of MOFs

The prepared Cr-MIL-101 and Fe-MIL-101-NH$_2$ materials were characterized by X-ray diffractometer (Model 7000, Shimadzu Corporation, Tokyo, Japan) equipped with a Cu-Kα radiation source (scanning range between 5° and 60° (2θ) at a step width of 0.02°) to analyze the crystal structure and composition. Brunauer–Emmett–Teller (BET) nitrogen adsorption method was used for the determination of specific surface area, and the pore size distribution was determined using the DFT model. Before the measurement, the MOFs materials were vacuum degassed for 6 h, and then the adsorption as well as desorption curve of nitrogen was measured at 77 K using a gas adsorption instrument (Autosorb iQ, Quantachrome Corp., USA). A zeta potentiometer (Zetasizer Nano ZS system, Malvern Instruments) was used to analyze the zeta potentials of material. The Fourier transform infrared (FT-IR) spectroscopy was recorded on Bruker Vertex 70 FTIR Spectrometric Analyzer using KBr pellets. Thermogravimetric analysis (TGA, UK) was carried out on a PerkinElmer TG/DTA thermo-gravimetric analyzer with a rate of 10 °C min^{-1} in nitrogen atmosphere at the range of 25–800 °C.

Sorption and regeneration experiments

Adsorption experiments were carried out at room temperature (25 °C) at pH 7.0 in glass flasks. Parallel experiments were performed in each set of experiments, and the data obtained were averaged. The results of blank controls indicated that the mass loss of adsorbates during adsorption process was negligible. A fixed amount of the adsorbents from 1 to 20 mg was added into the flasks. The sorption kinetic experiments of TPhP on different adsorbents were conducted at an initial concentration of 3.06 μmol L^{-1}. To obtain the sorption isotherms, the test solutions of the solutes at various concentrations (0–4.9 μmol L^{-1}) for TPhP were prepared by spiking the stock solutions into the background solution containing 200 mg L^{-1} NaN$_3$ to avoid any possible biodegradation. The solution amounts in the both adsorption kinetics and equilibrium experiments were 480 mL. After equilibrium (48 h), 5.0 mL of the mixed samples were withdrawn from each vial and filtrated using a 0.45 μm polyethersulfone (PES) membrane (the first 3.5 mL of the filtrate was discarded). The analysis of control experiments showed that the sorption of TPhP on the PES membrane was insignificant (recovery > 99%). For the experiment of pH effects, the solution pH was adjusted to be 3.0–9.0 using HCl and NaOH. To prepare the MOFs loaded with TPhP, the MOFs materials were added

into the TPhP solution, and the detailed adsorption conditions were controlled to be consistent with that of sorption kinetic experiments. After adsorption, the adsorbent materials were separated from the solution and vacuum dried.

In order to evaluate the selectivity of Cr-MIL-101 for TPhP and study the mechanism of selective adsorption, the removal of TPhP was compared with that of other OPFRs and several common aromatic compounds. In single solute experiments, the initial concentrations of different OPFRs and aromatic compounds were same (3.06 μmol L^{-1}). In double solute experiments, bezafibrate, phenol, 2,4,6-trimethylphenol with the same initial concentration were mixed with TPhP. To make all sorbates reach the adsorption equilibrium, the whole adsorption time was 48 h.

For the regeneration experiments, 5 mg of Cr-MIL-101 adsorbent was added into TPhP solution with initial concentration of 4.9 μmol L^{-1} and the solution was shaken for 24 h. After adsorption, the adsorbent material was filtered and collected, then regenerated in 50 mL of methanol for 24 h. The regenerated adsorbent was reused for the above adsorption process, and the whole experimental procedure was cycled for 5 times.

Analytical method

The concentration of OPFR was determined by high performance liquid chromatography-tandem mass spectrometry (LC-MS/MS). API 3200 triple quadrupole mass spectrometer (AB SCIEX, ON, Canada) connected with an UltiMate 3000 HPLC (Dionex by Thermo Fisher Scientific Inc., MA, USA) was used for detection. The volume of injection sample was 50 μL. The initial mobile phase was 40% methanol containing 10 mM ammonium acetate for 1 minute. A gradient ramp followed over 6 min to 100% methanol, which was held for 3.5 min, and then balanced in 40% methanol for 2.5 minutes. The more detailed HPLC-MS/MS running parameters were described elsewhere.[16] The concentrations of bezafibrate, phenol and 2,4,6-trimethylphenol were analyzed by HPLC (Shimadzu LC-2030, reversedphase C18 column, 5 μm, 4.6 mm × 250 mm, Japan) with a diode array detector operated at different wavelengths. Isocratic elution was used to determine the concentration at a flow rate of 1 mL min^{-1} with a mobile phase consisted of 70% methanol and 30% water.

Computational method

The MOFs adsorption complexes (ACs) models were built in Materials Studio 7.0, and geometry optimization was supported by Vienna *ab initio* simulation package (VASP). The crystal structure of Cr-MIL-101 material used in this study was obtained from the Cambridge Crystallographic Data Centre (CCDC), and because of the complexity of its structure, only one basic structural unit was used to calculate the adsorption energy. In the DFT calculations, a 25 × 25 × 25 Å^3 grid box was built. After the convergence test, the encut value was set to be 520 eV, and the threshold was set as 10^{-6} eV. Binding energies ($\Delta E_{binding}$) between Cr-MIL-101 and different sorbates were calculated by the following formula:

$$\Delta E_{\text{binding}} = E(\text{AC}) - E(\text{B}) - E(\text{Cr-MIL-101})$$

where B is the optimized energy of sorbate, and AC represents the total energy of the adsorption complexes.

Results and discussion

Characterizations of MOFs

The structure and composition of Cr-MIL-101 and Fe-MIL-101-NH$_2$ were analyzed by X-ray diffraction (XRD), and the patterns are illustrated in Fig. S1.† Significant characteristic absorption peaks of Cr-MIL-101 were at 5.8°, 8.4°, 9.0° and 16.4° (Fig. S1a†), while the peaks of Fe-MIL-101-NH$_2$ appeared at about 5.98°, 8.54°, 9.08° and 16.54° (Fig. S1b†). The peak patterns and the positions of the characteristic peaks were basically same to the reported studies,[28,29] indicating the successful preparation of the MOF crystal structures. It can be also seen that the characteristic peaks of Cr-MIL-101 and Fe-MIL-101-NH$_2$ were sharp, suggesting the high crystallinity of both two prepared MOF materials. The specific surface areas of MOFs were determined by BET nitrogen adsorption method, and the results are clearly shown in Fig. S2 and Table S2.† The type of nitrogen adsorption curves of Cr-MIL-101 and Fe-MIL-101-NH$_2$ were between type I and IV,[30] indicating that the materials had microporous and mesoporous structures. Table S2† showed that the prepared Cr-MIL-101 and Fe-MIL-101-NH$_2$ possessed large specific surface areas, and specifically the specific surface areas as well as pore volumes of Cr-MIL-101 were higher than Fe-MIL-101-NH$_2$ and commercial activated carbon in this study. Pore size distribution of Cr-MIL-101 and Fe-MIL-101-NH$_2$ materials is shown in Fig. 2. It can be found that both Cr-MIL-101 and Fe-MIL-101-NH$_2$ materials had large pore volumes at the pore width range between about 1 nm and 3.5 nm. Compared with Fe-MIL-101-NH$_2$, the pore volume of Cr-MIL-101 at 1–3.5 nm pores was almost twice as that of Fe-MIL-101-NH$_2$, consistent with their specific surface areas. Based on the pore size analysis (Fig. 2), two peaks of distribution were found at the pore size ranges of 1–2 nm and 2–3.5 nm, respectively, which is close to the cavity sizes (2.9 and 3.4 nm) of MIL-101 calculated from its crystal structure. It can be concluded that Cr-MIL-101 and Fe-MIL-101-NH$_2$ prepared in this study had both microporous structures (less than 2 nm) and mesoporous structures (2–3.5 nm), and this also explained why the nitrogen adsorption–desorption curve produced a hysteresis loop.[31]

The FT-IR and TGA analysis were also conducted, and the results are shown in Fig. 3. It can be seen from the FT-IR spectra that Cr-MIL-101 and Fe-MIL-101-NH$_2$ had strong bands at 1460 cm^{-1} and 1260 cm^{-1}, corresponding to symmetric O–C–O vibrations.[32] The bands observed between 600 and 1240 cm^{-1} were due to benzene ring,[33] including the deformation vibrations (C–H) at about 1104, 1018, 890, and 750 cm^{-1} (Fig. 3a). Different from Cr-MIL-101, Fe-MIL-101-NH$_2$ showed a FT-IR peak around 3400 cm^{-1}, which was attributed to the vibration adsorption of the N–H group.[34] The band from 1640 to 1700 cm^{-1}, assigned to the characteristics of C=O group, was not found in the FT-IR spectra of both MOFs.[35] It indicated that the pores of MIL-101 materials almost did not contain DMF solvent and H$_2$BDC or H$_2$BDC-NH$_2$ ligand molecules.

As shown in Fig. 3b, Cr-MIL-101 displayed three stages of weight loss during the heating process. The first stage of weight loss at 40–150 °C corresponded to the removal of water molecules in the macropores. The second stage of gravity loss (150–300 °C) might be also due to the removal of guest water molecules in the mesopores.[36] The weight loss, in the range of 300–600 °C, was about 40%, which might result from the decomposition of the framework. The major difference of TGA curves between Fe-MIL-101-NH$_2$ and Cr-MIL-101 was that the weight loss of Fe-MIL-101-NH$_2$ was much lower than Cr-MIL-101, probably due to the lower specific area of Fe-MIL-101-NH$_2$ for water adsorption from atmosphere.

Sorption kinetics and isotherms

The adsorption kinetics of prepared Fe-MIL-101-NH$_2$ and Cr-MIL-101 were compared with commercial activated carbon (Fig. 4). At the beginning of the adsorption, the three materials adsorbed TPhP fast and the adsorption amount increased rapidly. When the adsorption time reached 12 h, the adsorbed amount on Cr-MIL-101 tended to be flat, indicating that the adsorption basically achieved an equilibrium. Comparatively, the adsorption equilibrium time of TPhP on Fe-MIL-101-NH$_2$ and activated carbon was much longer, more than 48 h (Fig. 4a). The kinetic data were fitted by the pseudo-second-order model (Table 1), and it is noted that the initial sorption velocity (v_0) of TPhP on the Cr-MIL-101 was much higher than other two adsorbents, suggesting that TPhP was more inclined to be adsorbed by Cr-MIL-101. The v_0 of TPhP on the adsorbents followed the order of activated carbon (105.04 μmol g^{-1} h^{-1}) <
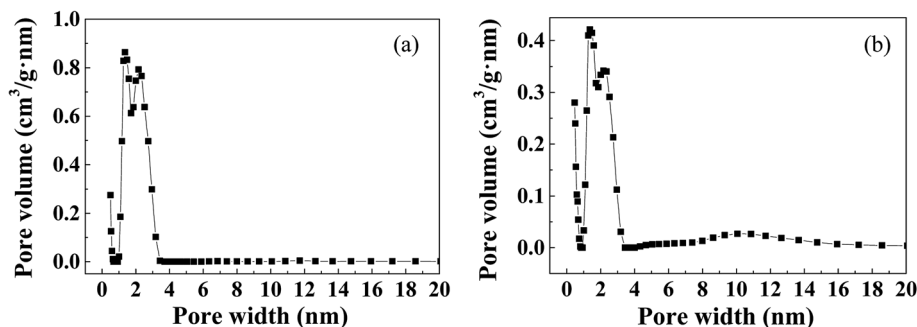

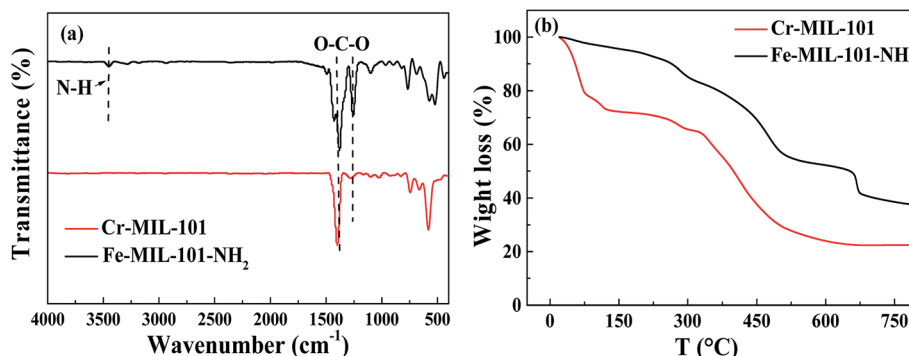Fig. 2 Cr-MIL-101 (a) and Fe-MIL-101-NH$_2$ (b) pore size distribution (DFT model).

Fig. 3 FTIR spectra of Cr-MIL-101 and Fe-MIL-101-NH$_2$ (a) and TGA curves of Cr-MIL-101 and Fe-MIL-101-NH$_2$ (b).

Fe-MIL-101-NH$_2$ (170.36 μmol g^{-1} h^{-1}) < Cr-MIL-101 (568.18 μmol g^{-1} h^{-1}) (Table 1), consistent with the sequence of their specific surface area values (Table S1†). The equilibrium adsorbed amount of TPhP by Cr-MIL-101 was also much higher than that of Fe-MIL-101-NH$_2$ and activated carbon. From the results of pore size distribution, Cr-MIL-101 had a greatly high pore volume at the pore size range (1–3.5 nm), which probably contributed to high capture capacity for TPhP whose maximum molecular diameter is approximately 1.14 nm (calculated by Gaussian 09 software). In comparison with the other reported absorbents (carbon nanotubes[15] and resins[16]), Cr-MIL-101 also possessed shorter adsorption equilibrium time, rapid sorption speed and higher sorption equilibrium amount for TPhP pollutant, implying that Cr-MIL-101 would be a promising adsorbent for TPhP removal.

Studies have shown that the adsorption process on porous adsorbent materials may mainly depend on intraparticle diffusion.[15] In order to further analyze the adsorption kinetics data of TPhP, the intraparticle diffusion model was used to fit the experimental data. The fitting results are shown in Fig. 4b and Table 1. According to the intraparticle diffusion model, the adsorption process of TPhP on three materials can be linearly fitted into two or three stages. In the first stage, the fitting straight line of TPhP adsorption on activated carbon almost passed through the origin with the very small value of c, suggesting that intraparticle diffusion may be the rate-limited step during the adsorption process on activated carbon. Cr-MIL-101

and Fe-MIL-101-NH$_2$ have the mesoporous cavities (2.9 and 3.4 nm), and thus the intraparticle diffusion of TPhP (about 1.14 nm) was faster (higher k_p, intraparticle diffusion rate constant) than activated carbon. In addition, the straight fitting lines of the two MOFs in the first stage did not pass through the origin, and the absolute values of c (Table 1) were much away from zero. This result demonstrated that the intraparticle diffusion was not the only rate-limited step to control the adsorption speed of TPhP on the MOF materials. In the second or the third stage, the values of c were higher than those in the first stage for all three adsorbents, but the slope values (k_p) became much smaller, suggesting that the adsorption became slower and the boundary layer diffusion might have comparable effects on the final sorption process.[37]

Adsorption isotherm can be used to describe the adsorption characteristics of sorbates and evaluate the adsorption performance of adsorbents. The adsorption isotherms of TPhP by three materials are illustrated in Fig. 5 and the data were fitted by Langmuir and Freundlich models (Table 2). As summarized in Table 2, both Langmuir model and Freundlich model could fit the adsorption isotherms of TPhP on all three adsorbents, but Freundlich model had higher correlation coefficients ($R^2 = 0.98$ and 0.99) for Cr-MIL-101 and Fe-MIL-101-NH$_2$ than Langmuir model. Langmuir model is based on the assumption that all the sorption sites present on sorbent surfaces have equal sorption affinity for solutes and monolayer coverage of adsorption has occurred on sorbent surfaces. Cr-MIL-101 and
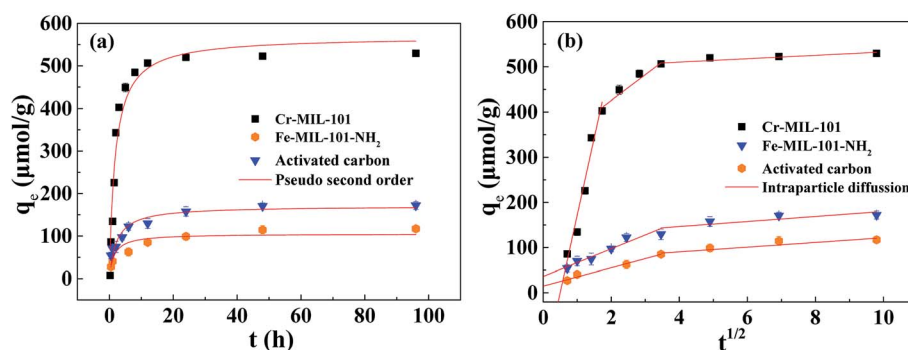

Fig. 4 Adsorption kinetics of TPhP and fitting results using the pseudo-second-order equation (a) and intraparticle diffusion model (b).

Table 1 Fitting parameters of the pseudo-second-order model and intraparticle diffusion model for adsorption of TPhP on adsorbents

Adsorbent materials	Pseudo-second-order parameters[a]			Intraparticle diffusion parameters[b]		
	q_e (µmol g^{-1})	v_0 (µmol g^{-1} h^{-1})	R^2	k_p (µmol g^{-1} h$^{-0.5}$)	c (µmol g^{-1})	R^2
Cr-MIL-101	312.50	568.18	0.96	342.3	−170.6	0.94
Fe-MIL-101-NH$_2$	76.86	170.36	0.90	30.5	36.3	0.92
Activated carbon	72.46	105.04	0.90	20.2	14.9	0.98

[a] Pseudo-second-order model: $t/q_t = 1/(k_2 q_e^2) + t/q_e = 1/v_0 + t/q_e$. [b] Intraparticle diffusion model: $q_t = k_p t^{1/2} + c$.
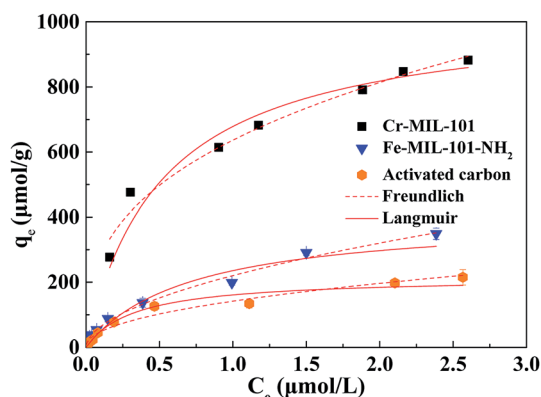
Fig. 5 Adsorption isotherms of TPhP on three different adsorbents and fitting results using Langmuir model and Freundlich model.

Fe-MIL-101-NH$_2$ consisted of benzene rings as well as metal oxide clusters, and apparently the sorption sites had different affinity for TPhP, which was unsuitable for the use of Langmuir model. Freundlich model is an empirical model, reflecting both monolayer and multilayer adsorption. Therefore, the better fitting by Freundlich model suggested that both monolayer and multilayer coverage of TPhP were probably involved in the adsorption on Cr-MIL-101 and Fe-MIL-101-NH$_2$. According to Freundlich model, the affinity coefficient (K_f) of Cr-MIL-101 sorbing TPhP was highest, exhibiting a higher adsorption affinity for TPhP compared to Fe-MIL-101-NH$_2$ and activated carbon. The calculated non-linear factors (n) of three adsorbents were 0.36–0.54, and thus the adsorption isotherm of TPhP was non-linear. It also indicated that chemical interactions occurred during TPhP adsorption process, probably responsible for the non-linearity of adsorption isotherms.[38] As shown in Fig. 5, when the concentration of TPhP increased at the lower

concentration range, the equilibrium adsorbed amount of TPhP increased greatly, but when the concentration continued to reach a certain level, the increase of TPhP adsorbed amount became gentle. Obviously, the adsorption amount did not become a relatively stable value, and thereby the adsorbents materials were not saturated at the whole TPhP concentration range in this study. Nevertheless, it can be still found that the maximum adsorption capacity of TPhP at such concentration range on three adsorbents decreased in the order of Cr-MIL-101 > Fe-MIL-101-NH$_2$ > activated carbon (Fig. 5), in agreement with the order of K_f value (Table 2). The maximum adsorption capacity of Cr-MIL-101 was about three times as that of Fe-MIL-101-NH$_2$, but the specific surface areas of Cr-MIL-101 were approximately twice as that of Fe-MIL-101-NH$_2$. Clearly, the adsorption sites on the surfaces of Cr-MIL-101 and Fe-MIL-101-NH$_2$ had different affinity for TPhP molecules. H$_2$BDC and H$_2$BDC-NH$_2$ were the organic linkers for Cr-MIL-101 and Fe-MIL-101-NH$_2$, respectively. NH$_2$ is a hydrophilic group and decreased the hydrophobicity of MOF surface as well as the potential hydrophobic attraction for TPhP, resulting in the lower adsorption capacity of Fe-MIL-101-NH$_2$. Besides, the inorganic building unit of Cr-MIL-101 and Fe-MIL-101-NH$_2$ is different, due to the different reactivity of their metals. Cr^{3+} is an inert cation, while Fe^{3+} is more active. The report found that the stability of Fe-MIL-101-NH$_2$ was poorer in water solution and the part of its structure was more ready to collapse, due to its higher reactivity.[29] This might lead to the lower adsorption for TPhP.

To further investigate the stability of two MOFs, the N$_2$ porosimetry, XRD, TGA and FT-IR analysis before and after TPhP adsorption at pH 7 were compared (Fig. S3–S7†). As shown in Fig. S3a,† adsorption of TPhP resulted in the disappearance of some bands and the weaker intensity of peaks in the XRD pattern of Cr-MIL-101. This may be caused by the load of TPhP

Table 2 Fitting parameters of adsorption isotherm models for TPhP

Adsorbent materials	Langmuir parameters[a]			Freundlich parameters[b]		
	q_m (µmol g^{-1})	b (L µmol^{-1})	R^2	K_f ((µmol g^{-1})/(µmol L^{-1})^n)	n	R^2
Cr-MIL-101	1030.12	1.93	0.95	636.47	0.36	0.98
Fe-MIL-101-NH$_2$	402.63	1.41	0.95	220.37	0.54	0.99
Activated carbon	215.25	2.95	0.98	141.54	0.47	0.96

[a] Langmuir model: $q_e = q_m C_e/(1/b + C_e)$. [b] Freundlich model: $q_e = K_f C_e^n$.

molecules on the Cr-MIL-101. The phenomenon is consistent with the report regarding the XRD change of MIL-101 after the adsorption of organic pollutant from the solution.[39] The characteristic peaks of Cr-MIL-101 at around 5.8°, 8.4°, 9.0° and 16.4° still existed, indicating that Cr-MIL-101 maintained good crystallinity. Comparatively, the XRD pattern of Fe-MIL-101-NH$_2$ changed greatly after adsorption (Fig. S3b†), suggesting the collapse of its crystalline structure.

As illustrated in the two FT-IR spectra (Fig. S4†), the intensity of infrared absorption bands became weak, probably due to the coverage of TPhP molecules on the adsorbent surfaces. The major spectra shapes of MOFs were not significantly changed. A new peak appeared around 1036 cm^{-1} (P–O),[40,41] indicating TPhP adsorbed on the both MOFs. Although the crystalline structure of Fe-MIL-101-NH$_2$ collapsed, most of surface groups still maintained after adsorption. TGA curves of Cr-MIL-101 showed significant difference between before and after TPhP adsorption (Fig. S5†). The decrease of weight loss below 380 °C after adsorption may be due to the decrease of water molecules. The adsorption of hydrophobic TPhP molecules could increase the hydrophobicity of Cr-MIL-101 and prevent Cr-MIL-101 from water molecules, decreasing the adsorption of water molecules. The weight loss of adsorbed TPhP may occur after 380 °C, because its boiling point is about 370 °C.[42] However, the TGA curve of Fe-MIL-101-NH$_2$ displayed a slight change after TPhP adsorption, probably due to the lower adsorbed amount of TPhP molecules. Comparing Fig. S6† and 2, it can been seen that the porosities of both MOFs decreased after TPhP adsorption. The major reason may be that the block of encapsulated TPhP in the pores decreased the determined pore volumes of MOFs. For Fe-MIL-101-NH$_2$, the collapse of the structure may also negatively influence its porosity. The specific area of MIL-101-Cr decreased about 23%, while that of Fe-MIL-101-NH$_2$ decreased above 45%. This may indicate the influence of pore collapse in the Fe-MIL-101-NH$_2$.

The stability investigation showed that Cr-MIL-101 was able to keep more stable in the solution than Fe-MIL-101-NH$_2$. From the adsorption kinetics and isotherms, it can be seen that Cr-MIL-101 had superior performance for TPhP, not only the sorption velocity but also the sorption capacity, to Fe-MIL-101-NH$_2$ and activated carbon. Therefore, Cr-MIL-101 was selected as the typical MIL-101 adsorbent for the following experiments.

Effect of solution pH

The effect of different pH values of solution on the adsorption of TPhP by Cr-MIL-101 material was studied (Fig. 6). The adsorption of TPhP by Cr-MIL-101 increased with the increase of pH from 3.0 to 9.0. When the pH increased from 6.0 to 7.0, the adsorption of TPhP on the Cr-MIL-101 increased most sharply. Surface properties of adsorbent and protonation of TPhP pollutant[43] in solution were affected by solution pH. The zeta potentials of Cr-MIL-101 at different pH values were measured (Fig. 6b). It can be found that the zeta potentials decreased gradually with the increasing solution pH, and the pH at the point of zero charge was about 6.53. Hence, the surface charge of MIL-101 was positive at pH values below 6.53 and negative at

pH values above 6.53. To our best knowledge, the specific pK_a value of TPhP is currently unavailable. But it has been reported that the pK_a values of phosphonic esters are commonly at the range of 6.1–16.4.[44] The estimated pK_a value of diethyl phosphite was reported to be about 13. As a similar type of phosphonic ester, TPhP (triphenyl phosphate) may possess a similar pK_a value. Besides, in the chemical structure of TPhP, the oxygen atoms on the phosphoric acid group have a high electron cloud density, so they have a strong affinity for protons in water, which makes TPhP easy to protonate at low pHs.[16] When the solution pH was low, the protonated TPhP had a positive charge, and there was probably electrostatic repulsion between the protonated TPhP and positive Cr-MIL-101, leading to the lower adsorption amounts. With the increase of solution pH, the amount of positive charge of Cr-MIL-101 decreased (Fig. 6b), resulting in the weaker electrostatic repulsion and the increase of TPhP adsorption.

To investigate the stability of Cr-MIL-101 in the basic solution, the XRD and FT-IR before and after TPhP adsorption at pH 9 were compared. It can be seen from the Fig. S7a† that the intensity of peaks in the XRD curve became weaker after adsorption at pH 9. But the characteristic peaks still maintained, suggesting that the crystalline structure may be preserved. Similarly, the FT-IR pattern showed the weaker intensity after adsorption at pH 9, which probably was due to the adsorption of TPhP. It has been reported that some Cr-based MOFs have a stable property in the basic solutions, since Cr^{3+} is an inert metal.[45] Nevertheless, it should be noted that the stability of Cr-MIL-101 may be a problem when it is used under basic conditions.

Effects of ion strength and organic solvent

NaCl and CaCl$_2$ were used to study the effect of ionic strength on the adsorption of TPhP by Cr-MIL-101, and the results are displayed in Fig. 7a. The removal of TPhP by Cr-MIL-101 increased with the increase of ion strength in NaCl and CaCl$_2$ solution. Comparing the effects of the two salts, it can be seen that TPhP removal increased slightly when the NaCl concentration increased in solution, consistent with the previous report that Na$^+$ had little influence on TPhP uptake.[16] However, the more significant influence made by CaCl$_2$ was found. Specifically, TPhP removal increased from 59.1% to 90.2% by Cr-MIL-101 with increasing Ca^{2+} concentrations from 0 to 5 mmol L^{-1}. The hydration of cations have influence on the aqueous solubility of hydrophobic organic compound. The solubility of hydrophobic organic compound declined after salts added, making more molecules separated from bulk solution onto the adsorbents, namely salting-out effect.[46,47] This may lead to the increase of hydrophobic TPhP adsorption with the increase of ion strength. According to the report,[48] phosphonic esters can be cationized by cations in the solution, which is similar to the protonation process, and may form [phosphonic ester + Na]$^+$ or [phosphonic ester + Ca]$^{2+}$, due to the high electron cloud density of oxygen atoms of phosphonic ester. Since Cr-MIL-101 has been reported to adsorb Ca^{2+},[49] Cr-MIL-101 may also adsorb the [phosphonic ester + Ca]$^{2+}$. In the
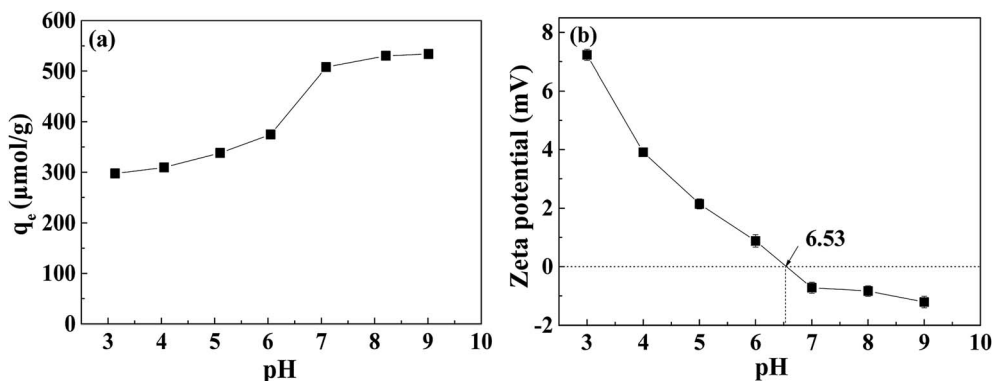
Fig. 6 Effect of pH on the adsorption of TPhP by Cr–MIL-101 material (a) and zeta potentials of Cr–MIL-101 at different pH values (b).

process, Ca^{2+} played a role of the bridge. This similar divalent cation-bridging effect has been widely reported,[50,51] which may explain the significant adsorption increase of TPhP after the addition of Ca^{2+}.

To further explore the hydrophobic interactions between TPhP and Cr–MIL-101, the effect of organic solvent on TPhP adsorption was also investigated using methanol. The removal of TPhP by Cr–MIL-101 in different solutions containing certain proportion of methanol is shown in Fig. 7b. As can be seen, the removal percentage of TPhP by Cr–MIL-101 decreased from 61.7% to 22.5% with the increasing proportion of methanol up to 10% in the mixed solution. It has been reported that Cr–MIL-101 presents a high affinity for methanol molecules.[52,53] The amount of methanol in the solution is greatly higher than that of TPhP, and the molecular size of methanol is smaller. Therefore, the adsorption sites might be occupied by methanol molecules during the adsorption process, making less TPhP adsorbed by Cr–MIL-101. In addition, with the change of methanol ratio, the solubility of TPhP in aqueous solution was influenced. Aromatic compounds have higher solubilities in organic solvent.[38,54] The solubility of TPhP in water is only 1.9 mg L^{-1},[14] while TPhP is much more soluble in methanol. Therefore, the solubility of hydrophobic TPhP in the solution increased with the presence of methanol. TPhP molecules preferred staying in the bulk methanol solution to being distributed to the Cr–MIL-101 solid.

Selective adsorption

TPhP are commonly detected with other types of OPFRs together in the aquatic environments. Thus, adsorption of different OPFRs on the Cr–MIL-101 was also studied. As shown in Fig. 8, the adsorbed amount of OPFRs on the Cr–MIL-101, except DPhP, decreased with the decrease of their log K_{ow} value, proving the dominant role of hydrophobic interactions. As listed in Table S1,† all five kinds of OPFRs have similar phosphorus functional groups, but different organic carbon
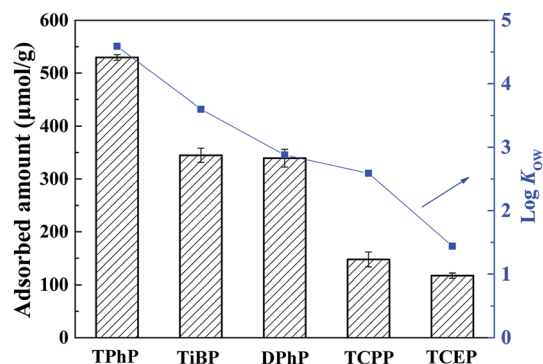

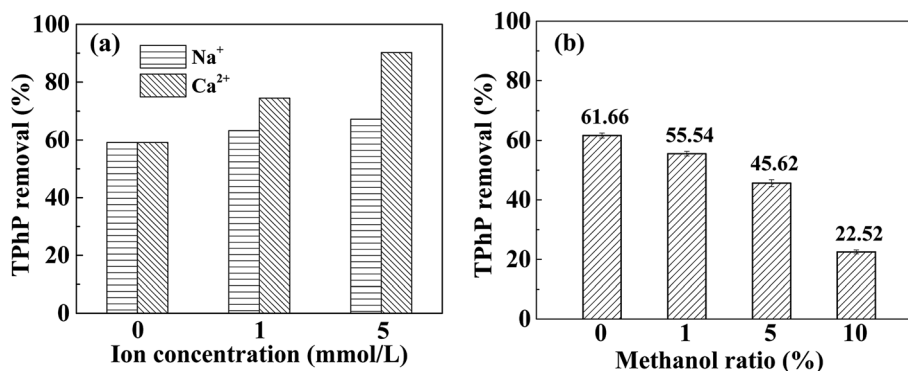Fig. 8 Adsorption of different OPFRs with their log K_{ow} on the Cr–MIL-101.

Fig. 7 Effects of ion strength (a) and methanol (b) on TPhP removal by Cr–MIL-101.

structures linked to phosphorus head. Although the log K_{ow} (3.6) of TiBP is much higher than that of DPhP (log K_{ow} = 2.88), the adsorbed amount of TiBP was only slightly higher than DPhP. Such result implied that other adsorption interactions, besides hydrophobic effects, might influence the adsorption process. The major difference between aromatic OPFRs (DPhP and TPhP) and alkyl-OPFRs is that the two aromatic OPFRs possess benzene rings which can generate π–π interactions with the benzene structures on Cr-MIL-101. Therefore, π–π interactions might also enhance the adsorption of aromatic OPFRs onto the Cr-MIL-101. It can be summarized that Cr-MIL-101 showed a better selective adsorption for aryl-OPFRs compared to alkyl-OPFRs.

To further explore the selectivity of Cr-MIL-101 for TPhP adsorption, three common aromatic compounds including phenol, bezafibrate and 2,4,6-trimethylphenol were selected for comparison. Those sorbates have different structures and chemical properties (Table S1†), and the Cr-MIL-101 material exhibited different adsorption ability for them (Fig. 9a). Cr-MIL-101 showed more excellent removal for TPhP than other compounds, and specifically the removal percent of TPhP was about 8-fold of that of phenol and 4-fold of that of 2,4,6-trimethylphenol. As listed in Table S1,† the log K_{ow} values which show the hydrophobicity of organic compound followed the order of phenol (log K_{ow} = 1.46) < 2,4,6-trimethylphenol (log K_{ow} = 2.73) < bezafibrate (log K_{ow} = 4.25) < TPhP (log K_{ow} = 4.59), consistent with their removal rates by the Cr-MIL-101 (Fig. 9a). This result indicated that the hydrophobic effects might play a dominant role on the selective adsorption of Cr-MIL-10l for TPhP compared to other aromatic compounds. The adsorption of TPhP on Cr-MIL-101 material in a double-solute system (bezafibrate, phenol and 2,4,6-trimethylphenol mixed with TPhP, repetively) was also conducted. It can be seen from Fig. 9b that the removal efficiency of TPhP by Cr-MIL-101 decreased very slightly in the presence of phenol and 2,4,6-trimethylphenol, in comparison with TPhP in single-solute solution. The TPhP removal had no obvious change when bezafibrate coexisted in the solution, whereas the removal of bezafibrate decreased significantly from 71.7% to 58.4% in such dual-solute solution. Clearly, the four aromatic compounds may share the partial sorption sites of Cr-MIL-101. Despite of the

both high K_{ow} values of TPhP and bezafibrate (Table S1†), the bezafibrate molecule has a larger molecular size than TPhP. Consequently, more significant steric hindrance made bezafibrate molecules lagging behind TPhP molecules during the competitive adsorption onto the sorption sites of Cr-MIL-101. All in all, Cr-MIL-101 could still maintain a stable selective adsorption and high removal efficiency for TPhP in mix-solute system with co-existing compounds.

In order to investigate and verify the selective mechanisms of TPhP adsorbed onto Cr-MIL-101, four sorption scenarios with corresponding binding energies of TPhP, bezafibrate, phenol, 2,4,6-trimethylphenol sorbed respectively on single unit of Cr-MIL-101 were calculated using VASP and are illustrated in Fig. 10. The molecules of all four pollutants were more close to benzene structures of Cr-MIL-101 than metal unit. The minimum distances between four compounds and the benzene structures were 2.821–3.296 Å, while those between four compounds and metal complex structures were from 3.083 to 4.005 Å. Even though the hydrophilic active sites (chromium oxo-clusters) on the framework of Cr-MIL-101 can chemisorb some water molecules and form hydroxyl groups which may further form hydrogen bondings with oxygen atoms in above four compounds, the bulk water molecules around the hydrophilic surfaces of metal clusters will cover the hydrogen-bonding sites for other compound molecules.[55] As shown in Fig. 10, the oxygen parts of compounds all were far away from the chromium oxo-clusters of Cr-MIL-101. Those results indicated that the major adsorption form of four different aromatic compounds mainly occurred on the hydrophobic benzene rings of Cr-MIL-101. Comparing the values of $\Delta E_{binding}$ calculated from four sorption scenarios, the $\Delta E_{binding}$ of TPhP on the Cr-MIL-101 was −0.069 eV, significantly higher than other pollutants, consistent with the results of the selective adsorption. TPhP is more hydrophobic, and its higher $\Delta E_{binding}$ value means the more stable adsorption system and higher binding affinity to Cr-MIL-101. The sequence of $\Delta E_{binding}$ values in different system followed as TPhP > bezafibrate > 2,4,6-trimethylphenol > phenol, which was same as the sequence of their log K_{ow} values. Above results proved that the hydrophobic interactions played the major role in the selective adsorption process. Besides, the
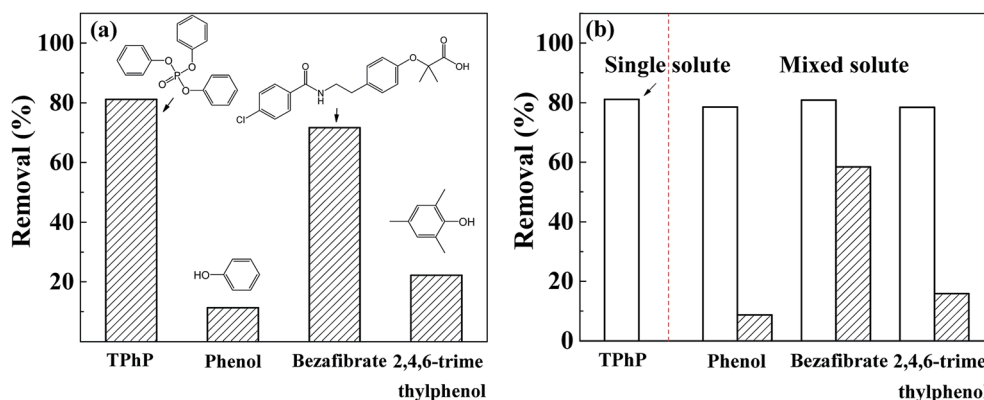

Fig. 9 Comparison of removal rates of TPhP by Cr-MIL-101 in single solute (a) and double-solute system (b).
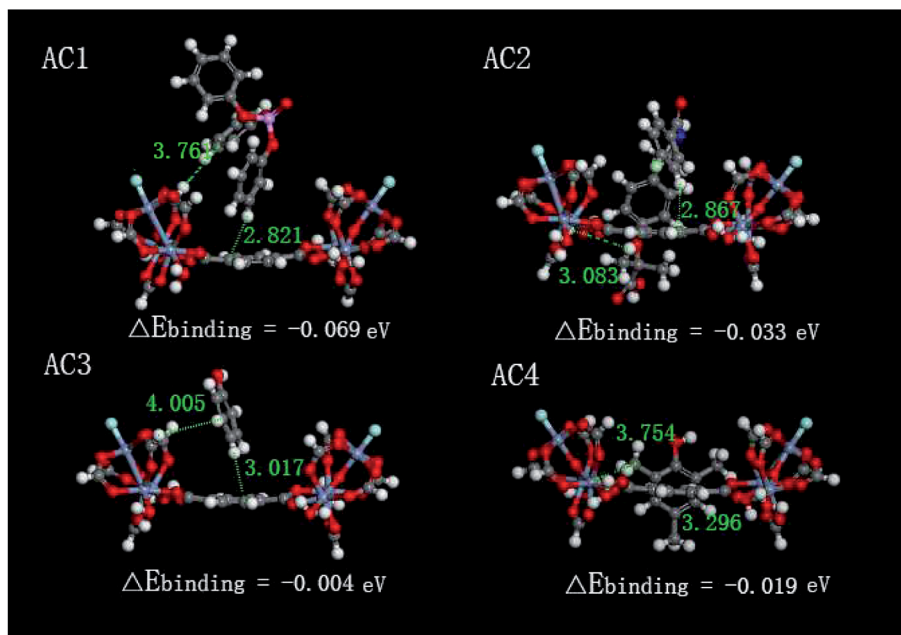
Fig. 10 Optimized conformations, binding energies and interatomic distances of MOFs adsorption complexes (ACs) (AC1, MOFs–TPhP; AC2, MOFs–bezafibrate; AC3, MOFs–phenol; AC4, MOFs–2,4,6-trimethylphenol; Cr, dark blue; C, grey; O, red; H, white; F, light blue; P, purple; Cl, green; N, cerulean).

adsorption morphologies of above four compounds displayed that all the benzene rings of pollutants were mainly vertical to the benzene plane of Cr-MIL-101 (Fig. 10), suggesting that π–π interactions occurring between two parallel benzene rings might not be the major role.

Regeneration of Cr-MIL-101

The regeneration and reuse properties of Cr-MIL-101 were evaluated using methanol as regeneration agent, and the regeneration efficiency as well as reuse of the adsorbent in 5 cycles were presented in Fig. S8 and S9.† It can be found that the regeneration efficiency of each time was not significantly reduced after reuse, and the values were between 93% and 97%. Obviously, methanol could desorb TPhP from Cr-MIL-101, basically in line with the decrease of TPhP adsorption in the methanol solution, as found in the former section. After the regeneration process, the material still maintained a high adsorption performance and exhibited a good reusability (Fig. S9†). Specifically, the Cr-MIL-101 showed a slight decrease (approximately 6.8%) in the adsorbed amount of TPhP after 5 cycles of reuse. The methanol as a regenerating solvent can be recovered and reused after distillation, thus reducing the cost of the actual adsorbent regeneration process.[56]

Conclusions

In this study, the MIL-101-based MOF adsorbent capable of rapid and efficient adsorption for TPhP was successfully prepared. MIL-101-based MOF possessed a high pore volume at the pore size range of 1–3.5 nm which was conducive to TPhP diffusion and adsorption. The initial adsorption velocity of Cr-

MIL-101 could reach 568.18 μmol g^{-1} L^{-1}, significantly faster than Fe-MIL-101-NH$_2$ and activated carbon. The TPhP adsorption equilibrium on Cr-MIL-101 was able to be basically achieved within 12 h, while the equilibrium time on Fe-MIL-101-NH$_2$ and activated carbon was more than 48 h. Cr-MIL-101 showed a better adsorption performance for TPhP than alkyl OPFRs and other aromatic compounds, and this performance could keep stable in the competition systems. The rapid, high and selective adsorption was attributed to the hydrophobic interactions and potential π–π interactions between TPhP and the benzene interfaces of Cr-MIL-101. Spent Cr-MIL-101 can be regenerated using methanol, and reused for several cycles with a high adsorption amount of TPhP. Cr-MIL-101 showed a good reusability, greatly rapid and selective adsorption for TPhP, and would be a promising adsorbent for the removal of aromatic OPFRs.

Conflicts of interest

There are no conflicts to declare.

Acknowledgements

References

1 R. Hou, Y. Xu and Z. Wang, *Chemosphere*, 2016, **153**, 78–90.
2 W. Wang, S. Deng, L. Ren, D. Li, W. Wang, M. Vakili, B. Wang, J. Huang, Y. Wang and G. Yu, *ACS Appl. Mater. Interfaces*, 2018, **10**, 30265–30272.
3 J. Regnery and W. Püttmann, *Water Res.*, 2010, **44**, 4097–4104.
4 C. Hao, P. A. Helm, D. Morse and E. J. Reiner, *Chemosphere*, 2017, **191**, 288.
5 G. Wei, D. Li, M. Zhuo, Y. Liao, Z. Xie, T. Guo, J. Li, S. Zhang and Z. Liang, *Environ. Pollut.*, 2015, **196**, 29–46.
6 Z. Du, Y. Zhang and G. Wang, *Sci. Rep.*, 2016, **6**, 21827.
7 X. Wang, J. Liu and Y. Yin, *J. Chromatogr. A*, 2011, **1218**, 6705–6711.
8 D. Canbaz, A. Logiantara, R. van Ree and L. S. van Rijt, *Chemosphere*, 2017, **177**, 56–64.
9 L. Feng, F. Ouyang and L. Liu, *J. Environ. Public Health*, 2016, **2016**, 1–7.
10 A. Blum, M. Behl and L. S. Birnbaum, *Environ. Sci. Technol. Lett.*, 2019, **6**, 638–694.
11 R. Hou, X. Luo, C. Liu, L. Zhou, J. Wen and Y. Yuan, *Environ. Pollut.*, 2019, **254**, 113040.
12 Q. Song, Y. Feng, Z. Wang, G. Liu and W. Lv, *Sci. Total Environ.*, 2019, **681**, 331–338.
13 J. Andresen and K. Bester, *Water Res.*, 2006, **40**, 621–629.
14 W. Wang, S. Deng, D. Li, L. Ren, D. Shan, B. Wang, J. Huang, Y. Wang and G. Yu, *Chem. Eng. J.*, 2018, **332**, 286–292.
15 W. Yan, L. Yan, J. Duan and C. Jing, *J. Hazard. Mater.*, 2014, **273**, 53–60.
16 W. Wang, S. Deng, D. Li, L. Ren, B. Wang, J. Huang, Y. Wang and G. Yu, *Chem. Eng. J.*, 2018, **354**, 105–112.
17 O. M. Yaghi, M. O'Keeffe, N. W. Ockwig, H. K. Chae, M. Eddaoudi and J. Kim, *Nature*, 2003, **423**, 705.
18 Y. Xiao, H. Huan, P. Ying, W. Xiao, G. Zhan, Y. Shao and S. Cheng, *Chin. J. Anal. Chem.*, 2012, **40**, 1693–1697.
19 H. Zhao, C. Hui, Z. Lei, H. Xuan, L. Wei, F. Wei and W. Guang, *Photochem. Photobiol.*, 2018, **94**, 512–520.
20 C. Ren, L. Cai, C. Chen, B. Tan, Y. Zhang and J. Zhang, *J. Mater. Chem.*, 2014, **2**, 9015–9019.
21 X. Wang and C. Deng, *Talanta*, 2015, **144**, 1329–1335.
22 H. Niu, S. Wang, Y. Tan, X. Song and Y. Cai, *RSC Adv.*, 2016, **6**, 99919–99923.
23 X. Li, H. Liu, X. Jia, G. Li, T. An and Y. Gao, *Sci. Total Environ.*, 2018, **621**, 1533–1541.
24 N. L. Torad, M. Hu, S. Ishihara, H. Sukegawa, A. A. Belik, M. Imura, K. Ariga, Y. Sakka and Y. Yamauchi, *Small*, 2014, **10**, 2096–2107.
25 M. Tong, D. Liu, Q. Yang, S. Devautour-Vinot, G. Maurin and C. Zhong, *J. Mater. Chem.*, 2013, **1**, 8534–8537.
26 G. Férey, C. Mellot-Draznieks, C. Serre, F. Millange, J. Dutour, S. Surblé and I. Margiolaki, *Science*, 2005, **309**, 2040–2042.
27 T. A. Vu, G. H. Le, C. D. Dao, L. Q. Dang, K. T. Nguyen, P. T. Dang, H. T. Tran, Q. T. Duong, T. V. Nguyen and G. D. Lee, *RSC Adv.*, 2014, **4**, 41185–41194.

28 Q. Yu, S. Deng and G. Yu, *Water Res.*, 2008, **42**, 3089–3097.
29 I. Y. Skobelev, A. B. Sorokin, K. A. Kovalenko, V. P. Fedin and O. A. Kholdeeva, *J. Catal.*, 2013, **298**, 61–69.
30 J. Möllmer, E. B. Celer, R. Luebke, A. J. Cairns, R. Staudt, M. Eddaoudi and M. Thommes, *Microporous Mesoporous Mater.*, 2010, **129**, 345–353.
31 Y. Chiang, P. Chiang and C. Huang, *Carbon*, 2001, **39**, 523–534.
32 S. Kayal and A. Chakraborty, *Chem. Eng. J.*, 2018, **334**, 780–788.
33 C. Petit and T. J. Bandosz, *J. Mater. Chem.*, 2009, **19**, 6521–6528.
34 A. D. Barbosa, D. Julião, D. M. Fernandes, A. F. Peixoto, C. Freire, B. de Castro, C. M. Granadeiro, S. S. Balula and L. Cunha-Silva, *Polyhedron*, 2017, **127**, 464–470.
35 S.-H. Choi and Y. C. Nho, *Radiat. Phys. Chem.*, 2000, **57**, 187–193.
36 Q. Liu, L. Ning and S. Zheng, *Sci. Rep.*, 2013, **3**, 2916.
37 W. Wang, A. Maimaiti, H. Shi, R. Wu, R. Wang, Z. Li, D. Qi, G. Yu and S. Deng, *Chem. Eng. J.*, 2019, **364**, 132–138.
38 Z. Du, S. Deng, Y. Chen, B. Wang, J. Huang, Y. Wang and G. Yu, *J. Hazard. Mater.*, 2015, **286**, 136–143.
39 E. Haque, V. Lo, A. I. Minett, A. T. Harris and T. L. Church, *J. Mater. Chem.*, 2014, **2**, 193–203.
40 A. Ślósarczyk, Z. Paszkiewicz and C. Paluszkiewicz, *J. Mol. Struct.*, 2005, **744**, 657–661.
41 I. Rehman, L. Hench, W. Bonfield and R. Smith, *Biomaterials*, 1994, **15**, 865–870.
42 K. Wei, H. Yin, H. Peng, G. Lu and Z. Dang, *Sci. Total Environ.*, 2018, **627**, 1389–1395.
43 J. Vank, H. Henry-Riyad and I. Csizmadia, *J. Mol. Struct.: THEOCHEM*, 2000, **504**, 267–286.
44 J. P. Guthrie, *Can. J. Chem.*, 1979, **57**, 236–239.
45 A. J. Howarth, Y. Liu, P. Li, Z. Li, T. C. Wang, J. T. Hupp and O. K. Farha, *Nat. Rev. Mater.*, 2016, **1**, 15018.
46 L. Tremblay, S. D. Kohl, J. A. Rice and J. P. Gagné, *Mar. Chem.*, 2005, **96**, 21–34.
47 H. Li, B. J. Teppen, D. A. Laird, C. T. Johnston and S. A. Boyd, *Soil Sci. Soc. Am. J.*, 2006, **70**, 1889–1895.
48 B. Fales, N. Fujamade, Y. W. Nei, J. Oomens and M. Rodgers, *J. Am. Soc. Mass Spectrom.*, 2011, **22**, 81–92.
49 A. A. Adeyemo, I. O. Adeoye and O. S. Bello, *Toxicol. Environ. Chem.*, 2012, **94**, 1846–1863.
50 F. Wang and K. Shih, *Water Res.*, 2011, **45**, 2925–2930.
51 L. Han, L. Qin, L. Xu, Y. Zhou, J. Sun and X. Zou, *Chem. Commun.*, 2013, **49**, 406–408.
52 M. F. De Lange, J. J. Gutierrez-Sevillano, S. Hamad, T. J. Vlugt, S. Calero, J. Gascon and F. Kapteijn, *J. Phys. Chem. C*, 2013, **117**, 7613–7622.
53 R. H. P. D. W. Green, R. H. Perry and D. W. Green, *Perry's chemical engineers' handbook*, McGraw-Hill Professional Pub, 2008.
54 R. Marcé and F. Borrull, *J. Chromatogr. A*, 2000, **885**, 273–290.
55 J. Zhang, L. Sun, C. Chen, M. Liu, W. Dong, W. Guo and S. Ruan, *J. Alloys Compd.*, 2017, **695**, 520–525.
56 J. Jin, S. Li, X. Peng, W. Liu, C. Zhang, Y. Yang, L. Han, Z. Du, K. Sun and X. Wang, *Bioresour. Technol.*, 2018, **256**, 247–253.